Acoustic Meta-Lens for Enhanced Sensing Consisting of Single-Helicoid Array

Li Xiang, Li Jian, and Huang Xinjing

***Abstract*—Magnifying lenses based on acoustic metamaterials (MMs) play an important role in many practical applications requiring acoustic focusing and amplification detection. However, the current 3D meta-lenses are still plagued by low flexibility, huge volumes, and high manufacture costs. We report a 3D meta-lens composed of discretely distributed meta-helicoid element that can solve the above problems. We improve the traditional helical MMs by reducing the number of blades to increase the distance between blades, achieving higher transmission efficiency and avoiding blade adhesion during manufacture. In order to eliminate the uneven phase and pressure of single-helicoid MMs at the outlet, pipe extension method is used to unify the phase and pressure. Via adjusting the spiral pitch, the meta-helicoid can generate 0-2π phase delay with a fixed outline size while maintaining transmittance greater than 90%. Based on the small single-helicoid meta-element, we design and manufacture a low-cost 3D magnify meta-lens with compact size. We demonstrate, both theoretically and experimentally, the acoustic meta-lens can make the normally incident signals focus on the prescribed point, enhances pressure amplitude about three times, and can flexibly manipulate focus point. Moreover, the bandwidth of the meta-lens is as wide as about 5.6 kHz. Our new strategy may offer an alternate route to the design of novel meta-lens and devices for acoustic focusing and amplification detection.**

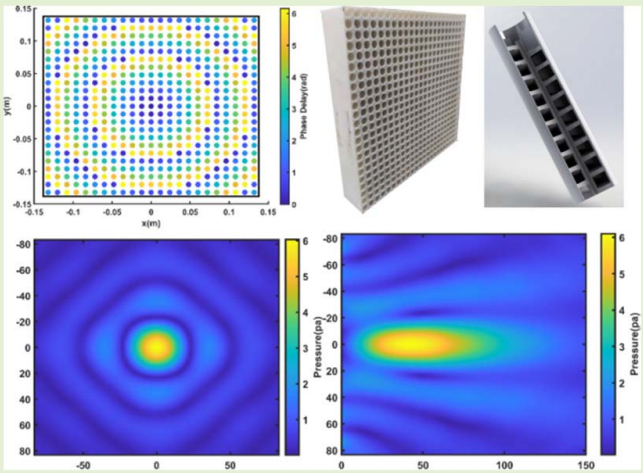

***Index Terms*— Acoustic focusing, metamaterial, meta-lens.**

I. Introduction

WITH acoustic focusing and amplification capacity, acoustic lenses have been applied in various scenes, such as underwater imaging [1]–[3], acoustic imaging [4], [5] and ultrasonic treatment [6], [7]. Conventional acoustic lenses [8]–[10] constructed by natural materials often have low amplification effect and coiled geometries, which limits their detection accuracy and application scope.

Since acoustic metamaterials (MMs) can have variable refractive index and mass density by adjusting internal parameters, they have provided alternative solutions to designing acoustic focusing lenses [11]–[13] with compact size, flattened shape, and high transmission efficiency. Several kinds of acoustic MMs approaches, inspired by optics, have been used to realize acoustic lenses. Locally resonant structure occupied a negative mass density when acoustic waves resonated with the structure, including periodically arranged Helmholtz resonators [14]–[16] and cavity structures [17], [18] etc. Locally resonant MMs have limitations in terms of their relatively small bandgaps. After that, many attempts have been made to design coiling-up [19]–[22] space MMs for the purposes of extending the travel distances of acoustic waves and reducing the effective acoustic speed, to induce these MMs into having relatively high refractive indices. In this way, the shortcomings of locally resonant such as narrow bandgaps, can be overcome. But most of them are only used to construct a 2D meta-lens [23]–[26], which heavily hamper practical application.

In 2015, a new type of helicoid-structured MMs [27] was proposed by Zhu *et al*. The MMs present non-dispersive high effective refractive index that is tunable through adjusting the helicity of structures. Different from previous studies, the effective mass density of air in the helicalstructured is much larger than the before coiling-up MMs. Shanjun *et al.* [28] improved on this basis and proposed gradient index helicoid MMs, which can modulate acoustic wavefront with

Manuscript received 20 May 2022; accepted 6 June 2022. Date of publication 16 June 2022; date of current version 14 July 2022. This work was supported in part by the National Key Research and Development Program of China under Grant 2018YFC0808600, in part by the National Natural Science Foundation of China under Grant 61803280, in part by the Natural Science Foundation of Tianjin under Grant 19JCQNJC01700, and in part by the Key Research and Development Program of Tianjin under Grant 19YFZCSY00190. The associate editor coordinating the review of this article and approving it for publication was Dr. Cheng-Yao Lo. *(Corresponding author: Huang Xinjing.)*

The authors are with the State Key Laboratory of Precision Measuring Technology and Instruments, Tianjin University, Tianjin 300072, China (e-mail: tjupipe@tju.edu.cn; huangxinjing@tju.edu.cn).

Digital Object Identifier 10.1109/JSEN.2022.3181981

nearly perfect transmission over a broad bandwidth. Analytical analysis of this helical-structured metamaterial with gradient-pitched element design can be resolved with the effective medium model and provide the possibility of inverse design from acoustic parameter distribution to its geometric parameter counterparts. Using the impedance characteristic of helicoid-structured MMs, Ding *et al.* [29] presented the concept of acoustic meta-coupler for broadband impedance match between two media with different impedances and cross sections. Fan *et al.* [30] proposed a configurable curved acoustic metasurface for acoustic cloaking and illusion, and the helical array is established to realize continuous acoustic manipulation. The advanced helicoid-structured MMs have the potential to eliminate the problems of large space occupancy and highcost of existing 3D amplification lenses [31], [32], and promote high focusing efficiency and bandwidth. However, these helical MMs adopts complicated four-helicoid structure, which has great adhesion risk and clearance difficulty for 3D printing when they are applied to 3D meta-lenses.

In this work, we propose a new type of meta-lens which can be used for acoustic focusing and amplification detection. We use the single-helicoid MMs as the meta-element of the meta-lens, which is an improvement of the helical MMs. Our proposed structure has higher transmission efficiency, and applies the pipe-extension method to unify the phase at outlet. Because the blade spacing is increased, when the meta-element of the meta-lens is processed by 3D printing technology, the adhesion of the blade will not occur, which is more conducive to processing and manufacturing. Based on the meta-elements formed by single-helicoid MMs, we design a high-performance 3D meta-lens. Through numerical and simulation experiments, we prove that this meta-lens can easily change the focus position, which has a great pressure amplification effect and ultra-wide frequency band. Based on this meta-lens, the acoustic focusing effect and amplification detection can be achieved.

II. Design and Test of MM

A. Helical Structure Design

The structure of the proposed single-helicoid meta-element is illustrated in Fig. 1 (a). The structure contains one single axisymmetric helical air tunnel which is formed by a spiral blade rotating around a central shaft coaxial with a cylindrical shell. The internal structure of the metamaterial is shown in Fig. 1 (b), and the acoustic propagation path is marked with a red dashed line. The diameter and the height of the helical structure are D and L, respectively. P is the pitch of thread. The diameter of the central shaft, and length of the extension part at the cylinder shell end are d and E, respectively. The extension part of the shell end is used to homogenize the phase of the acoustic wave at the outlet. The helical channel is filled with air. Fig. 1 (c) shows the picture of one single-helicoid MM. The whole structure is made of photopolymer resin via 3D printing and satisfies with the acoustic hard boundary condition.

The actual propagation path L_a of the sound in the spiral channel is calculated as follows:

$$L_a = \sqrt{(\pi D_e)^2 + P^2} \tag{1}$$

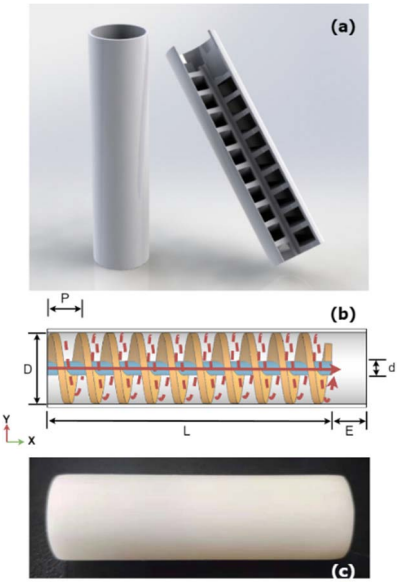

Fig. 1. Helical structure of the proposed MM: (a) schematic of the helical structure; (b) airborne acoustic path (red dotted arrow), equivalent straight path (red line arrow), and geometric parameter definition; (c) picture of one single-helicoid MM.

wherein D_e is the equivalent diameter of the spiral airborne path, and $D_e \approx 0.46D$. The equivalent path of the sound directly propagating from one end to the other is given as:

$$L_e = P \tag{2}$$

According to the effective medium theory, we can regard MMs as homogeneous meta-fluids with the same volume. If we deduce the effective refractive index of meta-fluids, we can easily calculate the phase-delays of MMs. The effective refractive index n_1 can be calculated as the ratio of the actual path length to the equivalent length:

$$n_1 = \frac{L_a}{L_e} = \frac{\sqrt{(\pi D_e)^2 + P^2}}{P} \tag{3}$$

Inside the helical MM, acoustic wave is forced to propagate along the helical path around the central axis instead of directly propagating in the axial direction. The actual curvilinear distance of adjacent wave crests inside the metamaterial is much larger than the straight-line distance along the axial direction, so the metamaterial having great effective refractive index. Therefore, the helical MM can adjust the effective acoustic speed and phase-shift of transmitted acoustic waves by adjusting the spiral pitch.

B. Simulation Test

Finite element method (FEM) simulation software COMSOL is employed to verify transmission coefficient and phase adjustment capacity of the single-helicoid MMs, and acoustic field homogenization capacity of the extension part. In order to ensure the accuracy of simulation, the mesh size of FEM simulation is less than one tenth of the wavelength. hexahedron structured meshing is used for the pipe part with regular structure, and tetrahedral free meshing is used for the metamaterial part with complex structure.

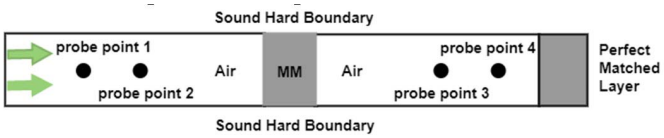

Fig. 2. Schematic of MMs simulation.

TABLE I
MM SIMULATION PARAMETERS

Parameter	Value	Description
D	10 mm	MM diameter
L	41 mm	MM length
d	2 mm	Shaft diameter
E	6 mm	Extension
ρ_1	$1.21\ Kg/m^3$	Density of air
C_1	$343\ m/s$	Velocity of air

The simulations were done in an impedance tube. The structural schematic of simulation model is shown in Fig. 2. An acoustic wave with an acoustic pressure amplitude of 1 Pa is incident from the left, and then the sound will propagate along the acoustic hard boundary pipe, pass through the test MM, and finally be absorbed by the perfect matching layer at the end. After calculation, the pressure of probe point 1, 2, 3 and 4 are collected to observe the acoustic field in the impedance tube after MMs is inserted into tube.

The performance of different number of blades is tested by replacing the MMs in the tube as shown in Fig. 2. The common parameters of two types of MMs are shown in Tab. I. The difference is whether they have a single blade or four blades, each of which rotates 90 degrees. Through parameter sweeping, we can easily calculate the transmissions and phase-delays of MMs as different pitch conditions according to acoustic pressure at four probe points.

Fig. 3(b) shows that the phase-delay as a function of the pitch increases with the pitch parameter increasing from 5 mm to 40 mm, in which the red solid line represents single-helicoid MMs, and the blue dotted line represents four-helicoids MMs. The results clearly show that for single-helicoid MMs, as the pitch increases from 8 mm to 31 mm, the phase delay can cover the entire 2π range. The pitch is increased from 10 mm to 38 mm to cover the entire 2π range for traditional spiral MMs. Both single-helicoid MMs and four-helicoid MMs can complete the control of the acoustic wave propagation path. The simulation result of intensity transmission is shown in Fig. 3(a). The average transmission (2π phase-delay range) of single-helicoid (red line) MMs is 90%, which is higher than the 76% transmission (2π phase-delay range) of four-helicoid MMs (blue dotted line). Therefore, the average transmission of single-helicoid MMs is 18.4% higher than that of traditional four-helicoid MMs in a compact size.

When we observe the outlet phase and pressure of cross-section, we can find that the output field has uneven pressure distribution and phase distribution. Fig. 4 (c) and (d) show the phase distribution of the MMs from outlet 0 mm and 6 mm, respectively. Fig. 4 (e) and (f) show the pressure distribution of the MMs from outlet 0 mm and 6 mm, respectively. Along the outlet pipe, the uneven field distribution gradually disappeared and unified into the same phase. As shown in Fig. 4. (a) and (b), with the continuous extension of the pipeline, the variance of the phase field distribution and the pressure field distribution continue to decrease. Since the nonuniformity of the discrete phase distribution will reduce the convergence of the meta-lens, the efficiency can be improved after the phase turn to uniform at the outlet. The method of guiding the acoustic wave to propagate a certain distance using the extension pipe can unify the distribution of the phase field and the pressure field. The extension part at the end of the single MM has great acoustic field homogenization capacity. The above conclusions are applied to the design and manufacture of meta-lens.

The simulation results of the MM and meta-lens are carried out under the assumption of lossless. We have simulated and analyzed the case with losses, and the simulation boundary conditions are the same as Fig. 2. Because the thermoviscous effect is significant in the narrow area, and the inserted MM will lead to the narrowing of the sound channel, with and without thermoviscous effect are compared in the MM area, in which the parameters are the actual parameters at room temperature of 23 °. The multi-physical field of acoustic thermoviscous interaction is used in simulation. Fig. 5 shows the transmission under different physical field conditions. we find that the intensity transmission is 100% at the peak point 1 of lossless transmission, and 94% at peak point 2 after adding thermoviscous losses, with a difference of only 6%. Therefore, the losses will not substantially affect the final result, and lossless conditions are used in both MMs and metalens simulations.

C. Experiment Test of Single MM

To further verify the actual performance of the single-helicoid MMs, experiment apparatus based on impedance tube shown in Fig. 6 (a) and (b). That is used to test its transmission and phase-delay manipulation ability. Impedance tubes are used to generate plane acoustic waves inside the tube while shielding out room noise. The sample being measured is held on sample tube between transmission tube and receiving tube. The joints between adjacent tubes and sample-tube are well sealed to minimize acoustic leakage. The back tube downstream the mic is filled with acoustic absorbing materials located at the end which is terminated by a well-sealed hard aluminum disk. The back impedance tube effectively shields the room noise, so that the measurements can be carried out in a normal laboratory instead of a specially equipped quiet room. Outputs of the mics are collected with NI DAQ board. We calibrated the impedance tube used in the experiment to make the result close to the simulation situation. The impedance tube adopts the classical method of four microphones to eliminate the influence of MM reflection and final terminal reflection on measuring amplitude and phase, and directly deduce the formula for calculating the transmissions and phase-delays [33]. At the same time, we tested and selected microphones to ensure the consistency of amplitude and phase.

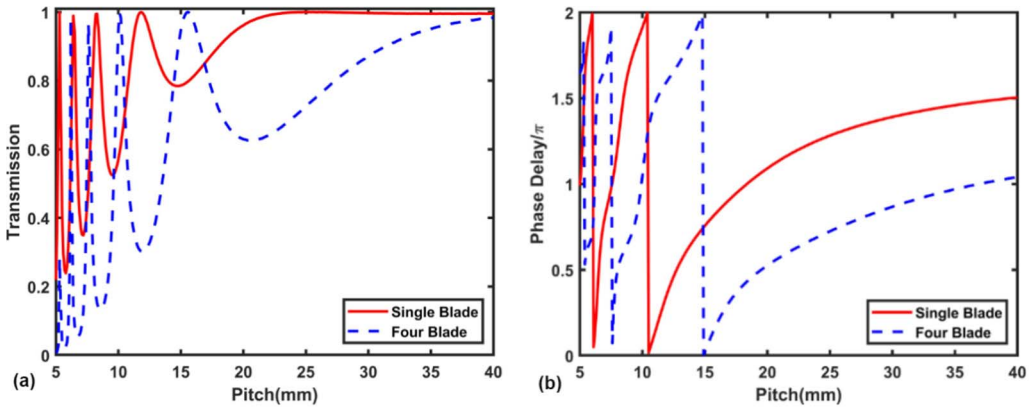

Fig. 3. Performance comparison of the helicoid MMs with different blade numbers: (a) transmission of single-helicoid MMs and four-helicoid MMs, as the pitch changes; (b) phase-delay of single-helicoid MMs and four-helicoid MMs, as the pitch changes.

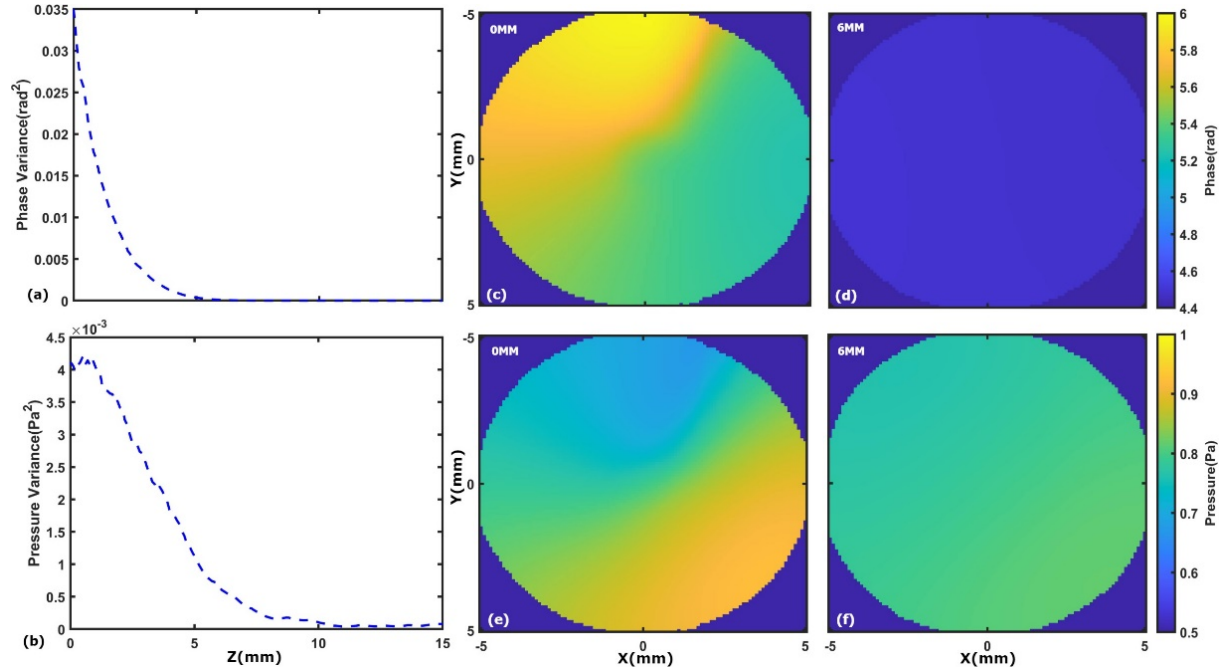

Fig. 4. Phase and pressure distribution at the outlet of the helicoid MMs: (a) and (b) the variance of the phase field and the pressure field with the extension of the guiding tube; (c) and (d) the phase distribution of the MMs from the outlet 0 mm and 6 mm, respectively; (e) and (f) the pressure distribution of the MMs from the outlet 0 mm and 6 mm, respectively.

Test results are shown in Fig. 7 (a) and (b). It can be seen that the simulation results are consistent with the experimental results, both in terms of pressure transmission efficiency and phase-delay, which proves that the single-helicoid MMs proposed in this paper has great energy transmission capacity. The experimental average transmission exceeds 80% and phase modulation of acoustic waves is consistent with the simulation. If the effective diameter is De = 0.46D, the theoretical phase-delays is in good agreement with the experiments and simulations.

III. Acoustic Magnifying Lens Design

As we all know, if the acoustic meta-lens is to converge acoustic waves at a fixed focal point, the phase of the acoustic waves from each meta-element propagating to the focal point should be the same, which means that there should be an elaborate phase-delay profile for the acoustic waves passing through each element of the meta-lens.

Assuming that the acoustic wave is transmitted along Z axis in the Cartesian coordinate system, as shown in Fig. 6 (a). The desired focal length is b. The refraction angle θ_t is closely related to the position of the meta-element, and the expression between x, y and $\theta_t$can be deduced as:

$$\sin(\theta_t) = \frac{\sqrt{x^2 + y^2}}{\sqrt{x^2 + y^2 + b^2}} \tag{4}$$

Since there is an exact phase delay along radial direction, the refraction angle can be deduced by the generalized Snell's law [34]:

$$\sin(\theta_t) = \frac{\lambda_0}{2\pi} \frac{d\varphi(x,y)}{dr} \tag{5}$$

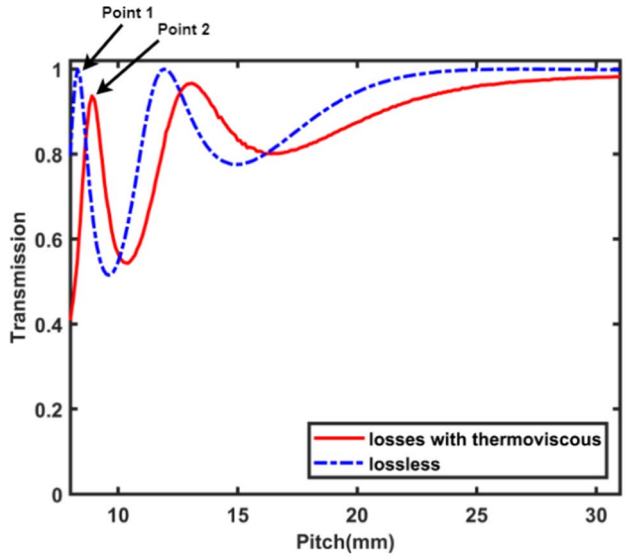

Fig. 5. With and without thermoviscous effect for transmission.

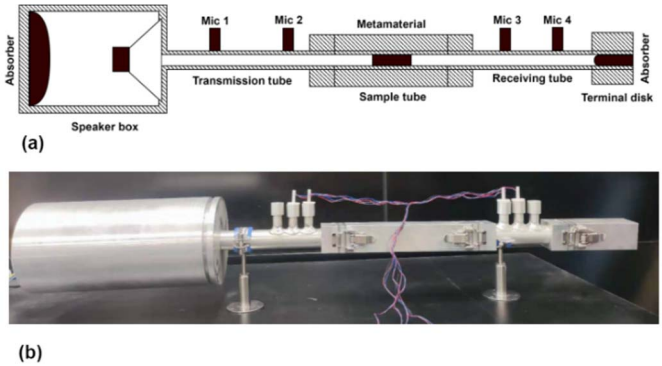

Fig. 6. MMs test experiment: (a) schematic diagram of impedance tube; (b) photo of transmission and phase-delay measurement experiment of single-helicoid MMs.

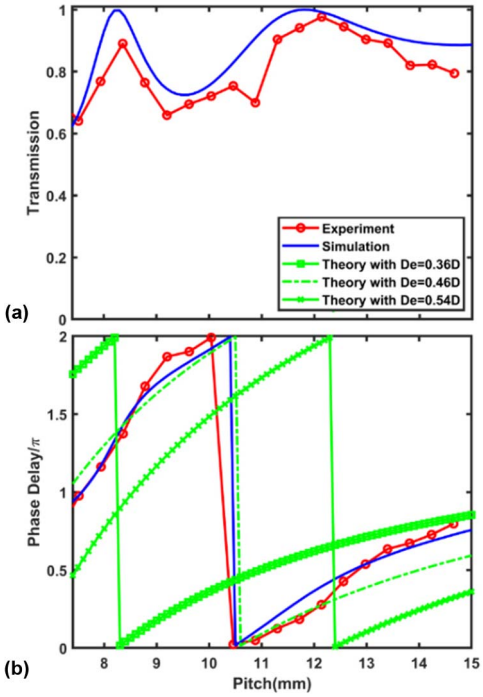

Fig. 7. Transmission (a) and phase-delay (b) comparison between analytical method, simulations and experiments.

wherein $\varphi(x,y)$ indicates the phase-delay across meta-elements along the radial direction. $\lambda_0 = \frac{c_1}{f}$ represents the wavelength of the acoustic waves in the air. $r = \sqrt{x^2 + y^2}$ represents the radius distance from the origin. Combining the two equations of (4) and (5), we can calculate the phase-delay of the meta-lens as follows:

$$\varphi(x, y) = k\sqrt{x^2 + y^2 + b^2} \tag{6}$$

wherein $k = \frac{2\pi f}{c_1}$ is wave vector in the air. It can be seen from equation (6) that the refraction angles can be realized by different phase-delays, and the phase distribution of the meta-lens should be symmetrical to the origin.

Since the single meta-helicoid element provides high transmission coefficient covered the entire 2π range, it can complete a meta-lens without worrying about the impact of low transmission. In order to obtain better convergence effect under compact size, we divide the planar lens into 23 row and 23 column regions. As is shown in Fig. 8 (b), the phase-delay profile of the meta-helicoid lens for focal length 50 mm is designed using a numerical method with equations (6), which makes the meta-elements along the X-axis and Y-axis meet the ideal phase-delay desired. To reveal the phase-delay in X-Y plane clearly, Fig 8 (d) and Fig 8 (e) show the ideal phase- delay (blue solid line) distribution along the radial direction (I) and X-axis direction (II), and the red dot represents the value of the discrete element.

Taking account of these extraordinary features, we designed and instantiated a thin flat meta-lens with an array of new meta-helicoid element, as is shown in Fig. 8 (c). The whole lens is composed of 529 independent elements, each discrete unit's diameter is only 10 mm, the overall height and width are 276 mm, and the thickness is only 47 mm. The spacing between the neighboring elements is 12 mm and all the elements are embedded in a holding frame. The phase modulation required by each element can be obtained by adjusting the pitch parameter. Because the phase-delay is linear, a relatively stable phase difference can be maintained between any two elements, which forms a uniform phase-delay profile. The application center frequency of the meta-lens we designed is 8.0 kHz to better observe the ultra wideband characteristic. Furthermore, using the design method in this paper, we can design meta-lenses with different center frequencies via changing the diameter of MMs.

IV. Numerical Simulations

A. Focusing Performances

The boundary conditions of meta-lens simulation are shown in Fig. 9 (a). The acoustic wave is incident into the pipe from the left and propagates in the form of plane wave in the pipe with acoustic hard boundary. Because the space behind the MM is surrounded by a perfect matching layer, the influence of reflection is avoided. In order to more intuitively represent the

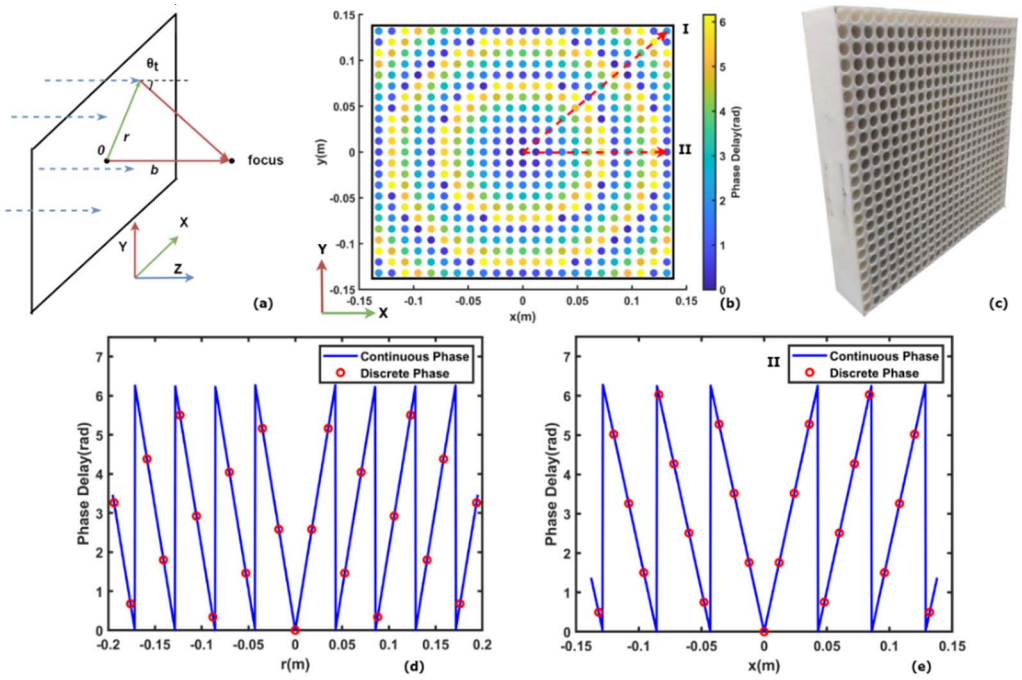

Fig. 8. Meta-lens design and its phase-delay distribution: (a) schematic diagram of acoustic waves propagating and converging; (b) discreted phase-delay distribution in meta-lens profile, where the red doted line I represents the distribution along the radial direction, and the red doted line II represents the distribution along the X-axis; (c) photograph of meta-lens; (d) phase-delay distributed along the radial direction in line I; (e) phase-delay distributed along the X-axis direction in line II.

TABLE II
META-LENS DIMENSIONS

Parameter	Value	Description
W	180 mm	Meta-lens width
H	180 mm	Meta-lens height
K	12 mm	Column spacing
I	12 mm	Row spacing
T	47 mm	Meta-lens thickness

pitch of the meta-lens unit at each position during simulation, the Fig. 9(b) shows the pitch of each position of the lens with a focal length of 20 mm. The parameters used in meta-lens simulation is shown in Tab II.

Transmitted acoustic pressure fields on the Z-X and X-Y planes obtained by FEM simulation at 8000 Hz are displayed in Fig. 10(a)(d) and (b)(e), respectively. It is found that the acoustic waves transmitting through the meta-helicoid lens converge into the ellipse region and the acoustic pressure of other regions is extraordinarily weak. Besides, the focus point is located at about z = 19 mm and z = 62 mm, which is close to the theoretical value of 20 mm and 80 mm. To reveal the performance of acoustic focusing clearly, acoustic pressure fields along transverse and longitude lines I/II/III/IV/VI/V are shown in Fig 10(c) and 10(f), respectively. It demonstrates that the redirected wavefront possesses a peak pressure near the designed focusing point.

To further quantify the focusing performance of the 3D meta-lens, the results in the free space are also displayed for comparison. With the meta-helicoid lens, the acoustic pressure focus at the peak of the focus reaches about 6 Pa, which is six times that in the free space. On the basis of the above results, we deduce that the proposed acoustic lens shows high focusing performance in 3D space and its full width at half maximum (FWHM) is smaller than wavelength. As a result, the 3D meta-helicoid lens proposed in this paper is an effective way to improve the resolution to meet the requirements of high precision acoustic focusing in 3D dimension. As the focusing effect exists on the right side of these acoustic lenses and close to the theoretical focal positions, we could design the transmitted acoustic meta-lens with different focal positions. Besides, with the increase of the focus length, we also find that the FWHM width slightly broadens in X-Y plane (from 0.55λ to 0.83λ). Therefore, meta-lens can provide high focusing quality with efficient concentration of the acoustic waves in the convergence area for different focusing lengths.

Different from the previous researches, the proposed 3D meta-lens adopts a highly discretized design, consisting of hundreds of discrete elements. This means that the meta-lens could move its focal point in 3D space by rearranging the distribution according to equations (6) without reprinting the 3D meta-lens totally with a new one.

B. Broad Working Bandwidths

We designed a 3D helicoid-lens with a focal length of 50 mm. Fig. 11 shows the distributions of the acoustic pressure field in the Z-X plane with incident acoustic waves of 7.0 kHz, 8.0 kHz, 9.0 kHz, and 9.6 kHz. The obvious acoustic focusing exists for all these frequencies, so the proposed meta-lens demonstrates high focusing performances in the range of a very wide frequency band. Besides, the focus position moves

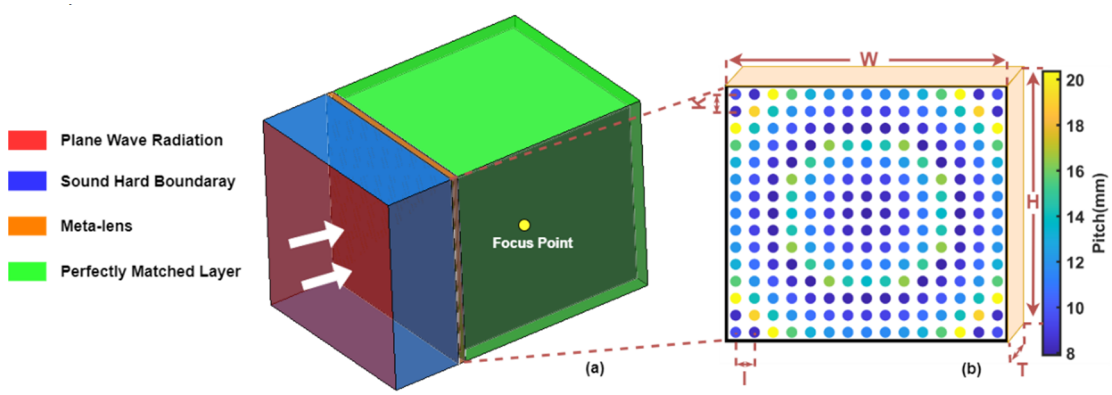

Fig. 9. Schematic of meta-lens simulation. (a) Structure and boundary conditions of meta-lens simulation. (b) Dimensions of meta-lens.

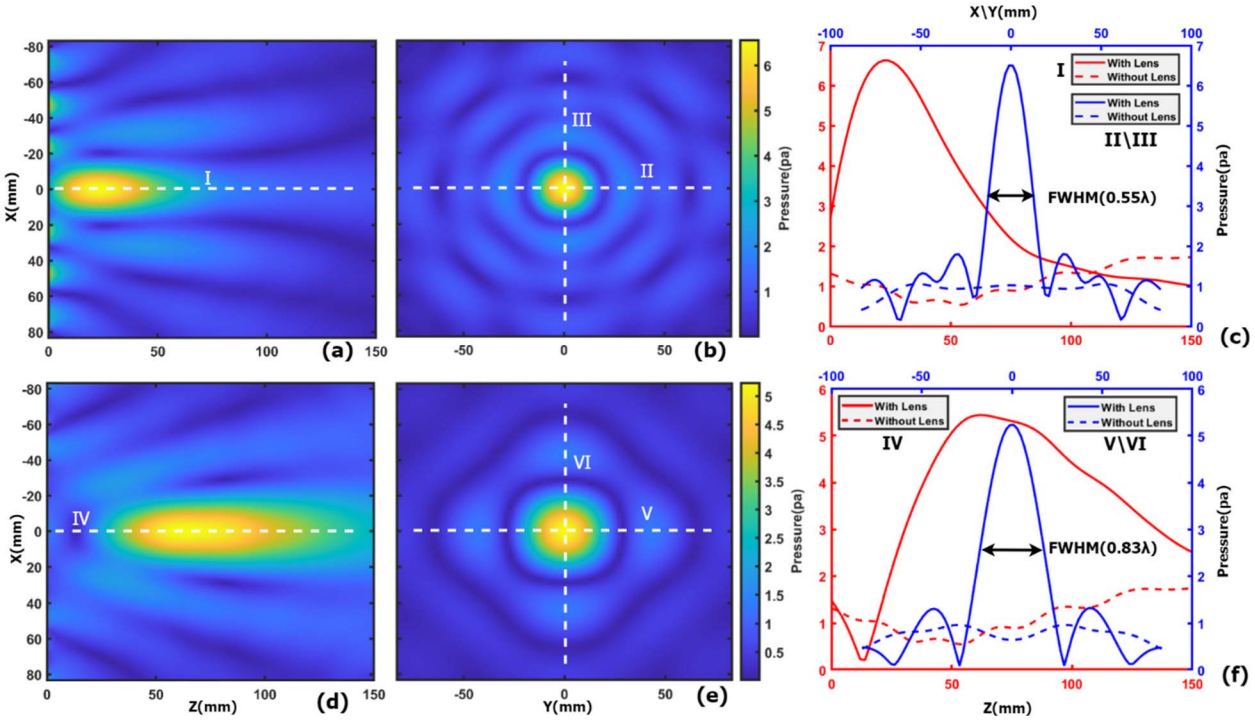

Fig. 10. Transmitted acoustic pressure field: spatial distributions of the acoustic pressure fields in the Z-X plane (a) and X-Y plane (b) induced by transmitted 3D meta-lens with a focal length of 20 mm, and with a focal length of 80 mm in the Z-X plane (d) and X-Y plane (e) at 8 kHz, respectively; distributions of acoustic pressure field along lines I and II\III (c), and along lines IV and V\VI (f) passing through the focus, respectively.

to the right slightly with the increase of the frequency, which means that meta-lens has similar distributions of the phase-delays under the broadband.

To further demonstrate the broadband performance of the acoustic lens, we calculate the Q factor defined as $Q = \frac{f_1}{\Delta f}$, where the parameters f_1 and Δf are the center frequency and bandwidth. Fig. 12 shows the pressure spectrum in the range from 5 kHz to 12 kHz. The parameters f_1 and Δf are about 8.3 kHz and 5.6 kHz, which indicates that the Q factor of the acoustic lens is about 1.48, very low. Therefore, we deduce that the proposed 3D meta-lens has the advantage of the broadband.

V. Experimental Verifications

The designed meta-lens is composed of a sample holder and 529 MM units that can be embedded inside. The units are inserted into the sample holder in a specific order, and the spacing between each meta-lens unit is 12 mm, as shown in Fig. 13.

Because the traditional manufacturing technology is difficult to process the meta-lens, we use photosensitive resin material to fabricate the meta-lens components through 3D printing technology. The density of the part processed with resin material is$1.13 g/cm^3$. As the application medium is air, the printing entity can regard it as the acoustic hard boundary.

Specifically, all parts of the meta-lens are made of resin material and processed by SLA (Stereolithography Apparatus) technology. It is an additive manufacturing technology, which can process the model of three-dimensional CAD into a solid. For a complex structure such as helicoid, the manufacturing time of the meta-lens unit is greatly shortened. The laser scans the photosensitive resin surface point by point in the liquid tank filled with liquid photosensitive resin according

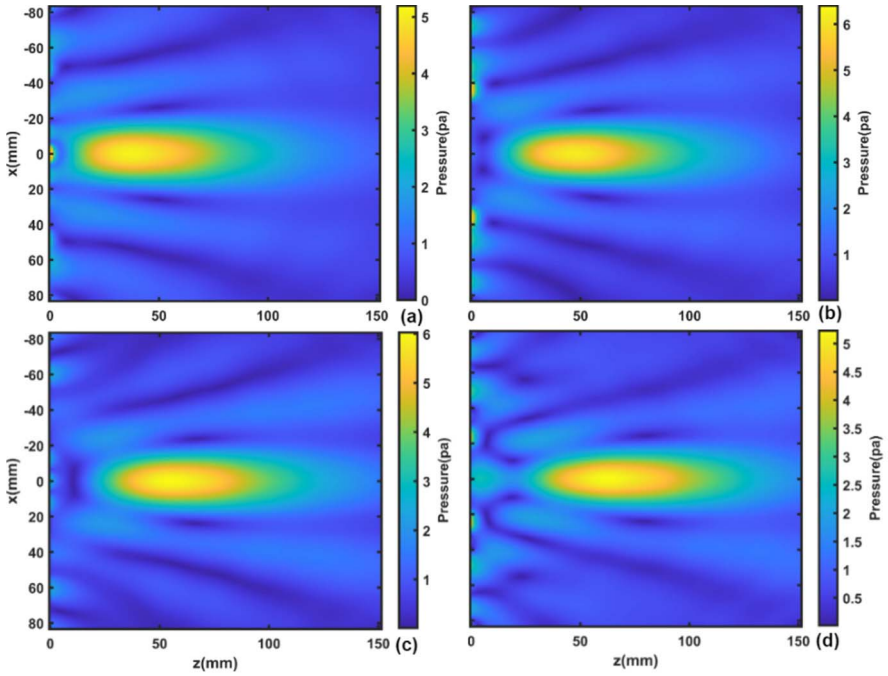

Fig. 11. Acoustic pressure field in the Z-X plane: (a) 7.0 kHz, (b) 8.0 kHz, (c) 9.0 kHz, and (d) 9.6 kHz.

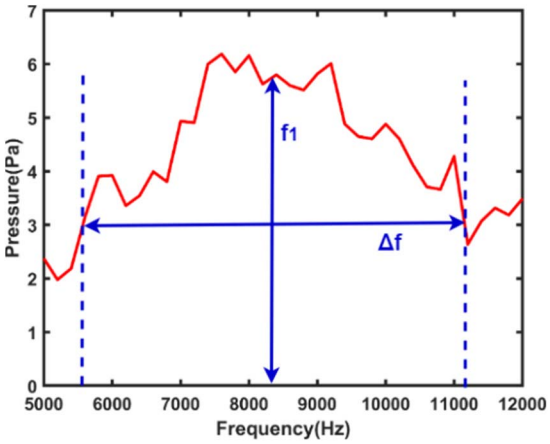

Fig. 12. Pressure spectrum ranging from 5 kHz to 12 kHz induced by the 3D meta-lens.

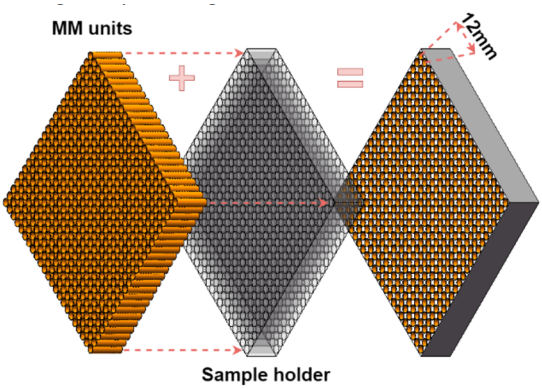

Fig. 13. Composition schematic of meta-lens.

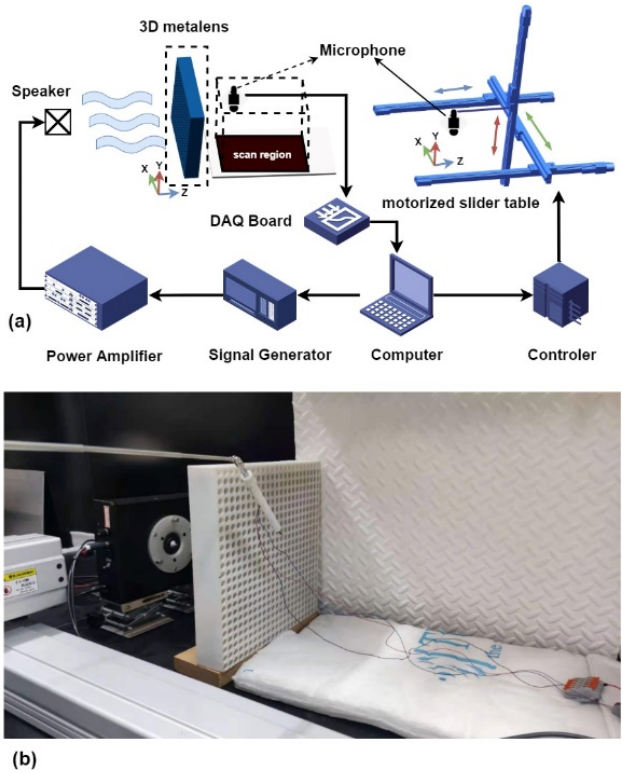

Fig. 14. Experimental apparatus: (a) schematic diagram of experimental devices (b) photo of experimental field.

to the layered section information, so as to solidify the resin thin layer in the scanned area. After one layer is cured, the workbench moves down to apply a new layer of liquid resin on the previously cured resin surface, and then scan the next layer after scraping. It is not difficult to see that after reducing the number of blades, the single-blade meta-helicoid element has a larger gap between the blades compared with the four-blade

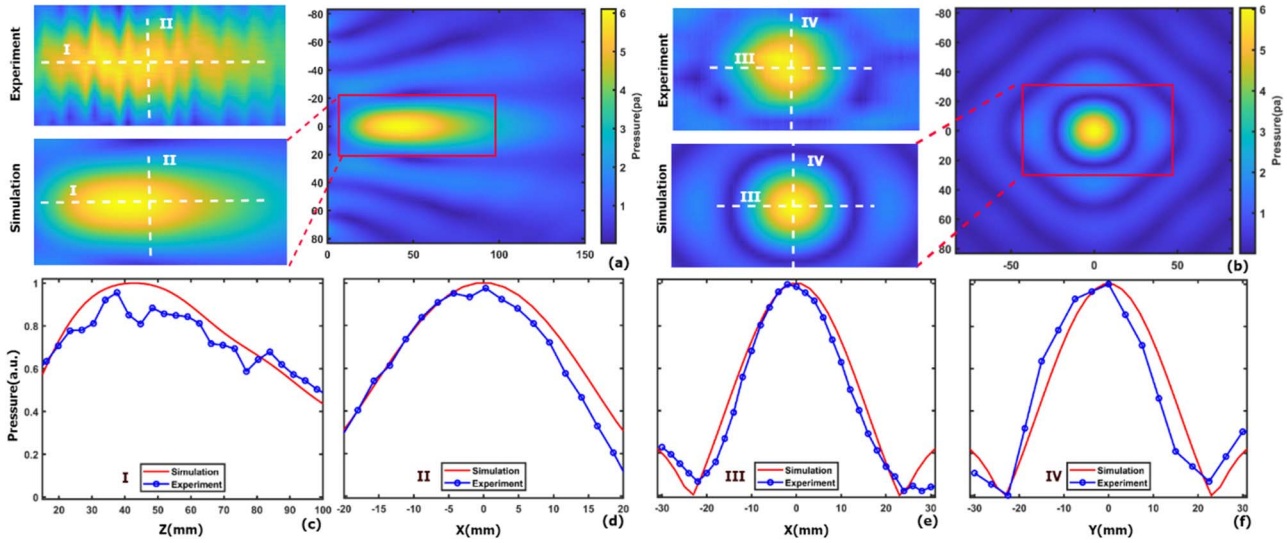

Fig. 15. Acoustic pressure field distributions obtained by simulation and experiment: (a) and (b) acoustic pressure field distributions on Z-X and X-Y planes, especially in the focus areas; (c) (d) acoustic pressure distributions along lines I and II on Z-X plane; (e) (f) acoustic pressure distributions along lines III and IV on X-Y plane.

meta-helicoid element, therefore structural adhesion during 3D printing can be avoided, and the redundant debris in the circulation channel can be easily cleaned up.

The experimental setup is shown in Fig. 14 (a). To realize an anechoic environment, acoustic absorbing foams are located aside as low reflectivity boundaries. The loudspeaker is used to radiate incident wave at one side of the acoustic meta-lens. A microphone is used for pressure field measurement, and the microphone is moved by a set of three-dimensional motorized linear stages to scan local pressures at different positions in the Z-X and X-Y plane. The data output by the microphone is recorded by the NI DAQ board and is analyzed by the LabVIEW software. Fig. 14 (b) is a picture of experiment field.

In Fig. 15, we compare the measured and simulated results of acoustic pressure. Fig. 15(a) shows the simulation results of the pressure fields in the Z-X plane, and the focus area is marked with a red frame. By comparing the experimental and simulated acoustic pressure fields in the focal region shown on the left, we can see that the experimental and simulated results are highly similar. In order to show the comparison results more clearly, we show the data of horizontal line I and vertical line II in Fig. 15(c) and (d), and it can also be seen that the experimental points overlap the simulation curves. Fig. 15(b) shows the simulation results of the pressure fields in the X-Y plane, and the focus area is marked with a red frame. By comparing the experimental and simulated acoustic pressure fields in the focal region shown on the left, we can see that the experimental and simulated results are highly similar. In order to show the comparison results more clearly, we show the data of horizontal line III and vertical line IV in Fig. 15(e) and (f), and it can also be seen that the experimental points almost overlap the simulation curves. This shows that the experimental results are highly close to the simulation results in the whole space field, which proves that the designed meta-lens has great acoustic convergence performance.

VI. Conclusion

In conclusion, we propose a new type of meta-lens to realize a 3D transmitted acoustic focusing and amplification detection with compact size. With a single blade, the new single-blade meta-helicoid provides higher transmission than four-blade meta-helicoid. As shown in simulation, average transmission is raised by 18.4%, and the adhesion during the process of 3D printing is avoided because of the structural simplification. With the pipe-extension method, we eliminate the uneven phase and pressure distribution at the outlet of the single-helicoid MMs. We model and fabricate a three-dimensional element lens composed of 23×23 helicoid MMs. The length and width of the meta-lens is 276 mm, the thickness is only 47 mm, and the diameter of each element is only 10 mm. Through numerical experiments, we prove that the meta-lens has great focusing effect and ultra-wide bandwidth of 5.6 kHz. To validate the performance of the meta-lens, we manufacture a meta-lens sample and design a set of experimental apparatus to measure distributions of the pressure field. In terms of amplification detection, it is experimentally demonstrated that it is in great agreement of pressure fields with the numerical results and enhance pressure amplitude about three times at the focal point. Our new strategy may offer an alternate route to the design of novel meta-lens and devices for acoustic focusing and amplification detection.

References

[1] H. Cho, B. Kim, and S.-C. Yu, "AUV-based underwater 3-D point cloud generation using acoustic lens-based multibeam sonar," *IEEE J. Ocean. Eng.*, vol. 43, no. 4, pp. 856–872, Oct. 2018.

[2] Y. Sato, K. Mizutani, N. Wakatsuki, and T. Nakamura, "Design for aplanatic Fresnel acoustic lens for underwater imaging," *Jpn. J. Appl. Phys.*, vol. 48, no. 7, Jul. 2009, Art. no. 07GL04.

[3] B. Kamgar-Parsi, L. J. Rosenblum, and E. O. Belcher, "Underwater imaging with a moving acoustic lens," *IEEE Trans. Image Process.*, vol. 7, no. 1, pp. 91–99, Jan. 1998.
[4] J. Chen, Z. Sun, J. Rao, D. Lisevych, and Z. Fan, "Escalated deep-subwavelength acoustic imaging with field enhancement inside a metalens," *Phys. Rev. A, Gen. Phys.*, vol. 16, no. 4, Oct. 2021, Art. no. 044021.
[5] J.-W. Kim, S.-J. Lee, J.-Y. Jo, S. Wang, and S.-H. Kim, "Acoustic imaging by three-dimensional acoustic Luneburg meta-lens with lattice columns," *Appl. Phys. Lett.*, vol. 118, no. 9, Mar. 2021, Art. no. 091902.
[6] G. Maimbourg, A. Houdouin, T. Deffieux, M. Tanter, and J.-F. Aubry, "3D-printed adaptive acoustic lens as a disruptive technology for transcranial ultrasound therapy using single-element transducers," *Phys. Med. Biol.*, vol. 63, no. 2, Jan. 2018, Art. no. 025026.
[7] X. Wu and M. Sherar, "Theoretical evaluation of moderately focused spherical transducers and multi-focus acoustic lens/transducer systems for ultrasound thermal therapy," *Phys. Med. Biol.*, vol. 47, no. 9, pp. 1603–1621, May 2002.
[8] M. Nishida, T. Endo, T. Adachi, and H. Matsumoto, "An acoustic lens to measure wave velocities with the complex V(z) curve method," *NDT E Int.*, vol. 32, no. 4, pp. 219–224, Jun. 1999.
[9] A. Atalar, I. Ishikawa, Y. Ogura, and K. Tomita, "Anisotropy sensitivity of an acoustic lens with slit aperture," in *Proc. IEEE Ultrason. Symp.*, Nov. 1993, pp. 613–616.
[10] D. Placko, T. Yanagita, E. K. Rahani, and T. Kundu, "Mesh-free modeling of the interaction between a point-focused acoustic lens and a cavity," *IEEE Trans. Ultrason., Ferroelectr., Freq. Control*, vol. 57, no. 6, pp. 1396–1404, Jun. 2010.
[11] C. Zhang *et al.*, "A reconfigurable active acoustic metalens," *Appl. Phys. Lett.*, vol. 118, no. 13, Mar. 2021, Art. no. 133502.
[12] F. Ma, Z. Huang, C. Liu, and J. H. Wu, "Acoustic focusing and imaging via phononic crystal and acoustic metamaterials," *J. Appl. Phys.*, vol. 131, no. 1, Jan. 2022, Art. no. 011103.
[13] Y. K. Chiang *et al.*, "Scalable metagrating for efficient ultrasonic focusing," *Phys. Rev. A, Gen. Phys.*, vol. 16, no. 6, Dec. 2021, Art. no. 064014.
[14] N. Fang *et al.*, "Ultrasonic metamaterials with negative modulus," *Nature Mater.*, vol. 5, no. 6, pp. 452–456, Apr. 2006.
[15] Y. Li, X. Jiang, B. Liang, J.-C. Cheng, and L. Zhang, "Metascreen-based acoustic passive phased array," *Phys. Rev. A, Gen. Phys.*, vol. 4, no. 2, Aug. 2015, Art. no. 024003.
[16] S. Tang, B. Ren, Y. Feng, J. Song, and Y. Jiang, "Broadband acoustic focusing via binary rectangular cavity/Helmholtz resonator metasurface," *J. Appl. Phys.*, vol. 129, no. 15, Apr. 2021, Art. no. 155307.
[17] J. Qian, J.-P. Xia, H.-X. Sun, S.-Q. Yuan, Y. Ge, and X.-Z. Yu, "Broadband acoustic focusing by cavity structures with phase manipulations," *J. Appl. Phys.*, vol. 122, no. 24, Dec. 2017, Art. no. 244501.
[18] Y. Han, J. Chen, and Z. Fan, "Broadband characterization of near-field focusing with groove-structured lens," *IEEE Access*, vol. 9, pp. 46061–46067, 2021.
[19] Z. Liang and J. Li, "Extreme acoustic metamaterial by coiling up space," *Phys. Rev. Lett.*, vol. 108, no. 11, Mar. 2012, Art. no. 114301.
[20] R. Ghaffarivardavagh, J. Nikolajczyk, R. Glynn Holt, S. Anderson, and X. Zhang, "Horn-like space-coiling metamaterials toward simultaneous phase and amplitude modulation," *Nature Commun.*, vol. 9, no. 1, pp. 1–18, Dec. 2018.
[21] Z. Jia, J. Li, C. Shen, Y. Xie, and S. A. Cummer, "Systematic design of broadband path-coiling acoustic metamaterials," *J. Appl. Phys.*, vol. 123, no. 2, Jan. 2018, Art. no. 025101.
[22] C. Liu, B. Xia, and D. Yu, "The spiral-labyrinthine acoustic metamaterial by coiling up space," *Phys. Lett. A*, vol. 381, no. 36, pp. 3112–3118, Sep. 2017.
[23] H.-X. Sun, J.-H. Chen, Y. Ge, S.-Q. Yuan, and X.-J. Liu, "Broadband and flexible acoustic focusing by metafiber bundles," *J. Phys. D, Appl. Phys.*, vol. 51, no. 24, Jun. 2018, Art. no. 245102.
[24] J. Li, L. Fok, X. Yin, G. Bartal, and X. Zhang, "Experimental demonstration of an acoustic magnifying hyperlens," *Nature Mater.*, vol. 8, no. 12, pp. 931–934, Oct. 2009.
[25] P. Peng, B. Xiao, and Y. Wu, "Flat acoustic lens by acoustic grating with curled slits," *Phys. Lett. A*, vol. 378, no. 45, pp. 3389–3392, Oct. 2014.
[26] H. Zhang, X. Zhou, and G. Hu, "Shape-adaptable hyperlens for acoustic magnifying imaging," *Appl. Phys. Lett.*, vol. 109, no. 22, Nov. 2016, Art. no. 224103.
[27] X. Zhu *et al.*, "Implementation of dispersion-free slow acoustic wave propagation and phase engineering with helical-structured metamaterials," *Nature Commun.*, vol. 7, no. 1, pp. 1–7, Sep. 2016.
[28] S. Liang, T. Liu, F. Chen, and J. Zhu, "Theoretical and experimental study of gradient-helicoid metamaterial," *J. Sound Vibrat.*, vol. 442, pp. 482–496, Mar. 2019.
[29] Y. Ding, E. C. Statharas, K. Yao, and M. Hong, "A broadband acoustic metamaterial with impedance matching layer of gradient index," *Appl. Phys. Lett.*, vol. 110, no. 24, Jun. 2017, Art. no. 241903.
[30] S.-W. Fan *et al.*, "Reconfigurable curved metasurface for acoustic cloaking and illusion," *Phys. Rev. B, Condens. Matter*, vol. 101, no. 2, Jan. 2020, Art. no. 024104.
[31] N. Korozlu and A. Cicek, "Compact acoustic lens composed of annular cavities covered by a membrane," *Appl. Phys. Lett.*, vol. 113, no. 18, Oct. 2018, Art. no. 183504.
[32] Y. Li *et al.*, "Three-dimensional ultrathin planar lenses by acoustic metamaterials," *Sci. Rep.*, vol. 4, no. 1, pp. 1–6, May 2015.
[33] L. Feng, "Modified impedance tube measurements and energy dissipation inside absorptive materials," *Appl. Acoust.*, vol. 74, no. 12, pp. 1480–1485, Dec. 2013.
[34] N. Yu *et al.*, "Light propagation with phase discontinuities: Generalized laws of reflection and refraction," *Science*, vol. 334, no. 6054, pp. 333–337, Oct. 2011.

Li Xiang received the M.E. degree from the Tianjin University of Technology, in 2018, where he is currently pursuing the Ph.D. degree with the Department of Instrument Science and Technology. His research interests include acoustic sensors and metamaterials.

Li Jian received the B.E., M.E., and Ph.D. degrees from Tianjin University, in 1994, 1997, and 2000, respectively. He is currently a Professor with Tianjin University. His research interests include pipeline leak detection and pipeline safety warning with acoustic methods.

Huang Xinjing received the B.S. and Ph.D. degrees from Tianjin University, in 2010 and 2016, respectively. He is currently an Associate Professor with Tianjin University. His research interests include structural health monitoring and damage detection for underwater infrastructure with acoustic and/or magnetic methods.